Identifying the prone zones to initiation of unstable failure by numerical simulation of mining pillars under compression

by A. Doroudgar[1] and H. Noferesti[1]

Affiliation:
[1]Faculty of Engineering, University of Birjand, Iran

Correspondence to:
H. Noferesti

Email:
hnoferesty@birjand.ac.ir

Dates:
Received: 10 Aug. 2022
Revised: 5 Feb. 2024
Accepted: Aug. 2024
Published: November 2024

How to cite:
Doroudgar, A. and Noferrsti, H. 2024. Identifying the prone zones to initiation of unstable failure by numerical simulation of mining pillars under compression. *Journal of the Southern African Institute of Mining and Metallurgy*, vol. 124, no.11, pp. 661–672

DOI:
http://dx.doi.org/10.17159/2411-9717/2265/2024

ORCiD:
H. Noferesti
http://orcid.org/0000-0003-0178-8429
A. Doroudgar
http://orcid.org/0009-0003-5213-0763

Abstract

Unstable rock failure or rock bursting is one of the most dangerous problems in deep hard rock mines. This type of failure, that occurs uncontrollably, is associated with a significant release of strain energy from the surrounding rock. In this study, the numerical simulation of unstable rock failure was carried out using the three-dimensional explicit Lagranian finite-volume finite difference method to identify the onset and location of unstable failure events in the model. On this basis, a numerical simulation of mine pillars with width-to-height ratios of 0.5, 2 and 3 was performed. A criterion was developed, based on the calculation of the elastic strain energy, to determine the prone areas for the initiation of rockburst in the models. The results of this study showed that, in softer loading systems, due to large amounts of stored elastic strain energy, an unstable equilibrium is established, which leads to the rapid transfer of strain energy to the rock in the form of violent failure. It was also found that the unstable failure starts at the corners and free surface of the model. The new criterion developed in this study may help predict the occurrence of rockbursts in slender pillars and the design of pillars to control human and financial losses caused by this phenomenon.

Keywords

mining pillars; rockburst; elastic strain energy; finite difference method

Introduction

Traditionally, in mathematical and numerical analyses for the design of surface or underground excavations, the stress-strength approach or safety factor has been given the main attention. If the safety factor is less than one or the permissible value, it is considered a failure, and then the design parameters are changed to prevent it. However, in actual deep mining practice, and based on many experiences, not all rock failures are considered dangerous. In some situations, deep underground miners deliberately create fractures in excavation walls or rock pillars to control ground stresses. By this logic, rock failures are divided into stable, which are safe and controllable, and unstable failures, which are uncontrollable and especially dangerous on a large scale. Based on the scale of this event, various names are given to the unstable failure phenomenon, including flaking, splitting, slabbing, and rock bursting.

As the mine depth increases, the in situ field stresses build up in the rocks. The mining activities cause the concentration of field stresses to increase to higher levels in the vicinity of underground excavations. As a result, in certain locations, the induced stress values are much higher than the stress level in situ. Very high-stress levels can cause sudden failure and a release of strain energy in a short period of time by throwing out rock fragments, or the so-called unstable rock failure or rockburst.

In the history of mining, various reports of unstable rock failure have been recorded at the mining pillars and stopes, which leads to the sudden outflow of debris and broken pieces into the work environment (Osterwald, 1962; Peperakis, 1958). So far, unstable rock failure has led to the instability of underground cavities, the total collapse of mining panels, and numerous physical and financial losses (Chase et al., 1995; Zingano et al., 2004).

Salamon (1970) conducted pioneering research that resulted in a stability criterion. This criterion determines whether the failure process occurs in a stable and non-violent manner or an unstable and violent manner. Since then, there has been a considerable amount of research conducted on the possibility of unstable failure, and several criteria have been proposed to classify and predict the severity of rockbursts (i.e., Barton et al., 1974; Russenes, 1974; Hoek and Brown, 1980; Kidybinski, 1981). While several criteria have been proposed for classifying and predicting rockburst intensity to provide a basis for the design of

excavation support, in practice, it has been found that applications of these criteria lead to inconsistent prediction results (Zhao et al., 2017). In addition, the suggested criteria have considered only the overall chance of this event at a particular mine site and cannot determine the exact location of rockburst in an underground excavation. In this paper, after reviewing the unstable failure theory, a new criterion is proposed that can be easily integrated into numerical models of underground excavations and has the potential to assist in the prediction of the location of rockbursts in mining pillars.

Unstable failure theory

The unstable failure of the rock is closely related to the definitions of brittle and progressive failure. Brittle failure is a common failure of rock during which the strain energy of the material is greatly reduced. In this type of failure, there is usually very little plastic strain. Progressive failure is a type of failure in which the fracture and damage continue until the new geometry of the material reaches equilibrium. As a result, this type of failure is time dependent.

The unstable failure of rock occurs in underground mines when brittle rock is subjected to high stress by relatively soft loading systems (Cook, 1965; Salamon, 1970). This instability will be accompanied by the transfer of the potential energy stored in the loading system to the volume of crushed rock until the entire system reaches a static equilibrium. The energy required to propagate and develop the unstable failure is derived from the excess energy released from the loading system during the failure process, which can neither be stored nor lost.

Rock failure typically occurs in a controlled quasi-static mode. However, if the stored strain energy of the external loading system is further applied to the failing rock, the failure can also acquire dynamic properties. If the loading system is shown to release more strain energy than can be stored or dissipated by the failing rock, then the system is said to be in unstable equilibrium (Garvey, 2013).

A new representation of the interaction between a rock specimen and the loading system in uniaxial compression is presented in Figure 1, based on Salamon's (1970) work. The rock sample and the loading system are demonstrated by elastic springs. The loading system is a linear spring with constant stiffness K_s, and the rock sample is considered a nonlinear spring with variable stiffness K_{ir}. Before the maximum rock strength, the rock sample is in static equilibrium with the loading system, i.e., the load F is applied to the rock by the loading system and vice versa.

Any small displacement, Δx, applied to the end of the rock specimen past the point of failure results in two changes: 1. a change of force on rock, $k_s \times \Delta x$, where k_s represents the stiffness of the loading system, 2. a change of force on the loading system, $K_{fr} \times \Delta x$, where K_{fr} represents the local slope of the post-failure force-displacement curve of the rock (Figure 2). If the loading system is softer than the rock specimen, i.e., $k_s < K_{fr}$, then the total load applied on rock is greater than the load applied on the system and a net unstable load on failing rock exists that causes a violently unstable failure.

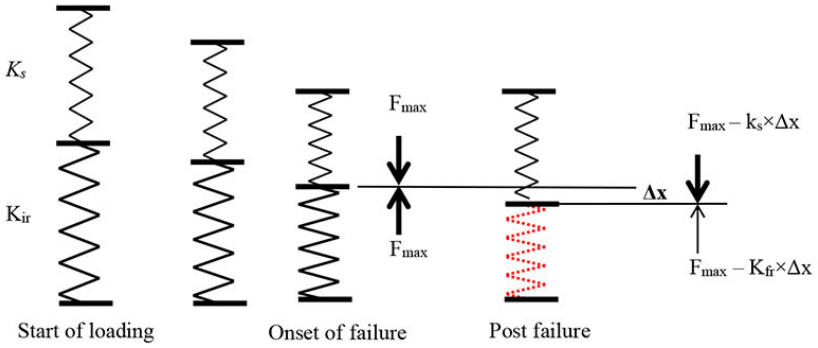

Figure1—Physical instability between an elastic soft loading system and brittle rock specimen (both depicted as springs) during the failure process

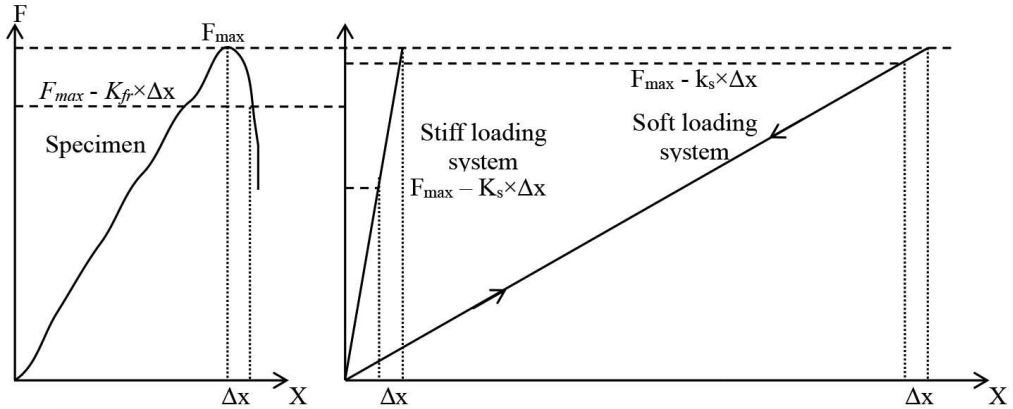

Figure 2—Force-displacement curves for soft/stiff loading systems and brittle rock specimen

As mentioned earlier, the phenomenon of unstable rock failure has also been studied in terms of energy balance. Once the failing process starts, both the rock system and loading system will release the stored strain energy, but the rate of release is different and dependent on their stiffness values. Unstable equilibria exist when brittle rock is loaded past the point of failure by a comparatively soft loading system. If the loading system stiffness is less than the post-failure stiffness of a rock sample and the peak strength of the rock is exceeded, then potential energy stored in the loading system will be transferred rapidly into the failing rock in the form of an unstable failure.

Based on theoretical and experimental studies on rockburst events in the laboratory and field, several criteria have been proposed to classify and predict the intensity of rockbursts. New comprehensive reviews of these criteria are provided by Bacha et al. (2020) and Askaripour et al. (2022). In a broad sense, these criteria can be divided into two categories: 1. based on energy, 2. based on stress. Various indexes are used in these criteria, out of which one energy index, i.e., W_{et}, and three stress indexes, i.e., σ_θ/σ_c, σ_c/σ_1, and σ_c/σ_v, are better known or accepted. The elastic strain energy index, W_{et}, was first proposed by Neyman et al. (1972) to categorize the intensity of the rockburst. The dimensionless value of this index is calculated as

$$W_{et} = \frac{E_e}{E_p} \quad [1]$$

Where E_e is the retained strain energy (elastic strain energy), and E_p is the dissipated strain energy. Both values are determined from elastic hysteresis loop parameters found in uniaxial compression loading and unloading tests.

The stress/strength index, σ_θ/σ_c, was first introduced by Russenes (1974) for classifying the intensity of rockburst events. This is where σ_θ and σ_c denote the tangential stress at the rockburst location and the uniaxial compressive strength of rock, respectively. Barton et al. (1974) introduced a strength/stress index, σ_c/σ_1, for the classification of rockburst severity. Here σ_1 denotes the major principal stress at the rockburst location. Another strength/stress index, σ_c/σ_v, was used by Hoek and Brown (1980) to estimate the damage potential of rockburst in underground mines. Here σ_v denotes the vertical stress at the mine location. Based on these four

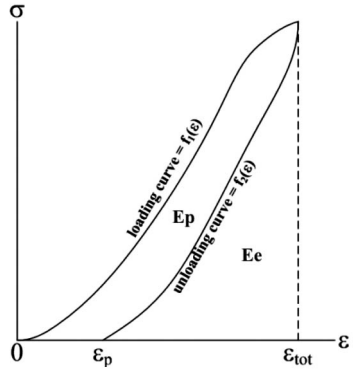

Figure 3—Stress-strain curves from loading-unloading uniaxial compression and the corresponding energy

indicators, many attempts have been made to classify the severity of rockbursts, usually into five categories: no, light, medium, heavy, and serious. Table I summarizes the different ranges proposed in this context. Subsequently, various other factors, including movement characteristics, sound characteristics, phenomenological characteristics, incision shape characteristics, time characteristics, and the degree of damage are employed to identify appropriate prevention strategies. Size of ejected fragments (d) is a factor that may be used as a rockburst descriptor: d < 10 cm for no rockburst, d = 10-30 cm for light rockburst, d = 30-80 cm for medium rockburst, d = 80-150 cm for heavy rockburst, and d > 150 cm for serious rockburst (Zhou et al., 2024).

Methodology

Developing a new criterion for identifying regions prone to unstable failure

As mentioned in the previous section, two approaches are followed in the study of unstable failure, i.e., the stress-strength approach and the energy balance approach. The stress-strength practice has been extensively developed in rock mechanics and used in various fields, such as experimental studies on rock, slope stability, and underground excavations. If the stresses on the rock overcome its strength, the rock fails.

Table I

Comparison between several criteria for rockburst classification

Rockburst classification	Index	No rockburst	Light rockburst	Medium rockburst	Heavy rockburst	Serious rockburst
Neyman et al. (1972)	W_{et}	< 2	2–3.5	3.5–5	> 5	
Russenes (1974)	σ_θ/σ_c	< 0.2	0.2–0.3	0.3–0.55	> 0.55	
Barton et al.	σ_c/σ_1	> 5	2.5–5		≤ 2.5	
Hoek and Brown	σ_c/σ_v	> 7	3.5	2	1.7	0.5
Kidybinski (1981)	W_{et}		< 2	2–5	> 5	
Tao (1988)	σ_c/σ_1	> 14.5	5.5–14.5	2.5–2.5	≤ 2.5	
Wang et al. (2009)	σ_θ/σ_c	< 0.3	0.3–0.5	0.5–0.7	> 0.7	
Zhang et al. (2003)	σ_c/σ_1	> 10	5–10	2.5–5	< 2.5	
Zhao (2017)	σ_θ/σ_c	≤ 0.2	0.2–0.5	0.5–0.7	0.7–0.9	> 0.9
Zhao (2017)	σ_c/σ_1	> 5	4–5	2.5–4	1.5–2.5	≤ 1.5
Zhou (2017)	W_{et}	< 2	2–5	5–10	> 10	

Although the rock failure could be predicted using the stress-strength approach, the type of failure, i.e., stable, or unstable, is better predicted by using the energy balance approach. Therefore, the energy approach is adopted in this paper, and an unstable failure index (UFI) is proposed as the ratio of elastic work performed on a rock unit (W) to the maximum stored (retained) elastic energy in the rock (Ee):

$$UFI = W/E_e \quad [2]$$

In the uniaxial compression test of a rock sample, the area below the stress-strain curve up to the peak point is equal to the maximum density of the elastic strain energy stored in the rock, and is obtained from Equation [3] (Brady and Brown, 2013).

$$e_e = ½\sigma\varepsilon \quad [3]$$

As mentioned, the unstable failure of the rock is closely related to the definition of brittle failure. Therefore, the behaviour of the rock, under unstable failure conditions up to the point of failure, can be assumed to be elastic. Also, given the maximum principal stress at the moment of failure, the elastic strain energy stored in the rock sample is:

$$E_e = V \cdot \left(\frac{1}{2}\sigma_1 \cdot \frac{\sigma_1}{E}\right) = V \cdot \left(\frac{\sigma_1^2}{2E}\right) \quad [4]$$

Where V is the sample volume and E is Young's modulus.
In triaxial compression, maximum storable elastic energy (E_e) in a rock sample is calculated using Equation [5] or [6]:

$$\begin{aligned} E_e &= V \cdot \left(\frac{1}{2}\sum \sigma_{ii}\varepsilon_{ii} + \sum \sigma_{ij}\varepsilon_{ij}\right)_{at\ Failure\ point} \\ &= V \cdot \left(\frac{1}{2}\left(\sigma_x\varepsilon_x + \sigma_y\varepsilon_y + \sigma_z\varepsilon_z\right) + \right. \\ &\quad \left.\left(\tau_{xy}\gamma_{xy} + \tau_{yz}\gamma_{yz} + \tau_{zx}\gamma_{zx}\right)\right)_{at\ Failure\ point} \end{aligned} \quad [5]$$

$$= V \cdot \left(\frac{1}{2}\left(\sigma_1\varepsilon_1 + \sigma_2\varepsilon_2 + \sigma_3\varepsilon_3\right)\right)_{at\ Failure\ point} \quad [6]$$

$$\varepsilon_1 = \frac{1}{E}\left(\sigma_1 - \upsilon(\sigma_2 + \sigma_3)\right), \quad [7]$$

$$\varepsilon_2 = \frac{1}{E}\left(\sigma_2 - \upsilon(\sigma_1 + \sigma_3)\right), \quad [8]$$

$$\varepsilon_3 = \frac{1}{E}\left(\sigma_3 - \upsilon(\sigma_1 + \sigma_2)\right), \quad [9]$$

Substituting the normal strains from Equations [7–9] in Equation [6]:

$$\begin{aligned} E_e = V \cdot \left(\frac{1}{2E}\right.&\left.(\sigma_1{}^2 + \sigma_2{}^2 + \sigma_3{}^2 - \right. \\ &\left.\left. 2\upsilon(\sigma_1\sigma_2 + \sigma_2\sigma_3 + \sigma_1\sigma_3)\right)\right)_{at\ Failure\ point} \end{aligned} \quad [10]$$

According to Mohr-Coulomb failure criterion, at failure point:

$$\sigma_1 = \sigma_c + \sigma_3 tan\psi = \frac{2cCos\varphi}{1-Sin\varphi} + \sigma_3\frac{1+Sin\varphi}{1-Sin\varphi} \quad [11]$$

Where c is the cohesion and ϕ is the angle of internal friction.

By applying the Mohr-Coulomb behaviour model to the rock sample, the maximum elastic strain energy that could be stored in the rock, is calculated using the relation [12] or [13] for 3D or 2D simulations, respectively:

$$\begin{aligned} E_e\ in\ 3D = V \cdot \left(\frac{1}{2E}\right.&\left.((\sigma_c + \sigma_3 tan\psi)^2 + \sigma_2{}^2 + \sigma_3{}^2 - 2\upsilon \right. \\ &\left.\left((\sigma_c + \sigma_3 tan\psi)\sigma_2 + \sigma_2\sigma_3 + (\sigma_c + \sigma_3 tan\psi)\sigma_3\right)\right) \end{aligned} \quad [12]$$

$$\begin{aligned} E_e\ in\ 2D = V \cdot \left(\frac{1}{2E}\right.&\left.((\sigma_c + \sigma_3 tan\psi)^2 + \sigma_3{}^2 - \right. \\ &\left.\left. 2\upsilon(\sigma_c + \sigma_3 tan\psi)\sigma_3\right)\right) \end{aligned} \quad [13]$$

On the other hand, the elastic work performed on the rock (W) in 3D and 2D can be calculated from the relations [14–15] using shear and normal stresses (Brady and Brown, 2013).

$$\begin{aligned} W\ in\ 3D &= V \cdot \left(\frac{1}{2}\sum \sigma_{ii}\varepsilon_{ii} + \sum \sigma_{ij}\varepsilon_{ij}\right) \\ &= V \cdot \left(\frac{1}{2}\left(\sigma_x\varepsilon_x + \sigma_y\varepsilon_y + \sigma_z\varepsilon_z\right) + \right. \\ &\quad \left.\left(\tau_{xy}\gamma_{xy} + \tau_{yz}\gamma_{yz} + \tau_{zx}\gamma_{zx}\right)\right) \end{aligned} \quad [14]$$

$$\begin{aligned} W\ in\ 2D &= V \cdot \left(\frac{1}{2}\sum \sigma_{ii}\varepsilon_{ii} + \sum \sigma_{ij}\varepsilon_{ij}\right) \\ &= V \cdot \left(\frac{1}{2}\left(\sigma_x\varepsilon_x + \sigma_y\varepsilon_y\right) + \left(\tau_{xy}\gamma_{xy}\right)\right) \end{aligned} \quad [15]$$

Substituting Ee and W from Equations [12–15] in Equation [2], a new criterion, Equations [16–17] is obtained, which indicates the areas susceptible to the onset of unstable failure in rock.

$$\begin{aligned} &UFI\ in\ 3D = \\ &\left[\frac{1}{2}\left(\sigma_x\varepsilon_x + \sigma_y\varepsilon_y + \sigma_z\varepsilon_z\right) + \left(\tau_{xy}\gamma_{xy} + \tau_{yz}\gamma_{yz} + \tau_{zx}\gamma_{zx}\right)\right] / \\ &\left[\frac{1}{2E}\left((\sigma_c + \sigma_3 tan\psi)^2 + \sigma_2{}^2 + \sigma_3{}^2 - \right.\right. \\ &\left.\left. 2\upsilon((\sigma_c + \sigma_3 tan\psi)\sigma_2 + \sigma_2\sigma_3 + (\sigma_c + \sigma_3 tan\psi)\sigma_3)\right)\right] \end{aligned} \quad [16]$$

$$\begin{aligned} &UFI\ in\ 2D = \\ &\left[\frac{1}{2}\left(\sigma_x\varepsilon_x + \sigma_y\varepsilon_y\right) + \left(\tau_{xy}\gamma_{xy}\right)\right] / \\ &\left[\frac{1}{2E}\left((\sigma_c + \sigma_3 tan\psi)^2 + \sigma_3{}^2 - 2\upsilon(\sigma_c + \sigma_3 tan\psi)\sigma_3\right)\right] \end{aligned} \quad [17]$$

According to Equation [2], UFI > 1 means that the work done on a rock unit is greater than the elastic strain energy stored in the rock. The excess energy can cause some kind of unstable failure unless it is absorbed by the plastic behaviour of the rock. Therefore, in a brittle rock that does not show plastic behaviour, UFI > 1 means the onset of unstable failure. As UFI increases from one, the severity of unstable failure increases. In general, UFI can be related to the widely studied W_{et} index to better estimate the onset of unstable failure. The minimum value of UFI above which unstable failure occurs is when the work done on a unit of rock is just equal to the maximum stored elastic energy plus the maximum strain energy dissipated in the rock:

$$UFI_{min} = \frac{W}{E_e} = \frac{E_e + E_p}{E_e} = 1 + \frac{E_p}{E_e} = 1 + \frac{1}{W_{et}} \quad [18]$$

There is an inverse relationship between UFI_{min} and W_{et} values. Rocks that are more brittle and have a higher W_{et} exhibit unstable failure at lower UFI_{min} values. Referring to Table I, and after using Equation [18], the minimum UFI for the onset of unstable failure are calculated as shown in Table II.

Previous criteria have been proposed only to classify and predict the intensity of rockbursts. However, the UFI index could be used in a numerical model to predict the rockburst's location (and intensity) around mining excavations. The next section presents an example of a UFI application in an FLAC3D model.

Table II

The relation between the W_{et} index of rock and minimum UFI for the onset of unstable failure

W_{et}	UFI_{min}
10	1.1
5	1.2
2	1.5

Simulation of unstable failure at mine scale

In this study, a finite difference numerical method, based on continuum mechanics, was used to simulate unstable failure and to evaluate the post-failure behaviour of a brittle rock at the mine scale, similar to the work of Garvey (2013). Then, the criterion that was developed in this paper was applied to the numerical models to evaluate its efficiency.

Numerical methods based on continuum theory provide powerful tools to predict rock mass failure. The finite difference method is widely and successfully used in the field of rock mechanics (Itasca, 2018). One of the main reasons for studying unstable failure by the finite difference is the explicit numerical formulation of this method by calculating the dynamic motion as a response to the physical instability in the model. Unlike finite element and boundary element methods, the explicit numerical formulation of the finite difference method can calculate the equilibrium of unstable forces by applying motion equations to determine the potential of large strain displacements in a continuous environment.

Mine pillar simulation

A mine pillar was simulated in a 2D plane strain condition to represent a coal pillar with its roof and floor rock masses. The height of the coal layer is set at 2.4 m, but the pillar width takes values from 1.2 m to 7.2 m in different simulations. Therefore, the pillar width-to-height ratio varied from 1:2 to 3:1. Two entries, 3 m wide, were created in the model on both sides of the pillar. On the outer sides of the entries, elastic sidewalls were modelled outward at about 40 m and were given elastic properties identical to pillar properties. A height of 80 m was given to the roof and floor rocks. The final model is shown in Figure 4. On the left and right sides of the model, roller boundary conditions were applied.

The primary aim of this paper was to develop a new identifier for unstable failure in mining (coal) pillars. The characteristics of the surrounding rock mass and rock-coal interface affect the pillar behaviour, but considering the aim of this paper, the failure was not allowed to progress in the surrounding elastic mass, and no slipping was allowed at the rock-coal interface. Also, for a proper comparison, the analyses were conducted using the same bord span of 3 m.

Previous studies on simulating brittle rocks in a continuous medium have used the Mohr-Coulomb strain softening behaviour model to represent the deformation and strength properties of the coal seams (Badr 2004; Hobbs and Ord 1989; Garvey 2013). Therefore, in this study, the Mohr-Coulomb strain softening law is applied to the pillar model. Another reason for using this behavioural model is to reveal the natural strength reduction of brittle rocks. For this study, the model developed by Garvey (2013), which had been calibrated using the empirical Mark-Bieniawski and Salamon-Munro formulas for pillar strength, was modified to perform UFI calculations and then used to reflect the behaviour of coal pillars. The initial coal cohesion was set to 1.45 MPa, while the initial friction angle was assumed to be 23 degrees. With the introduction of a 0.0005 plastic strain, cohesion was varied with a drop rate of –60 MPa/strain. The assumption was made that the friction and dilation angles would increase when plastic deformation is introduced. Young's modulus and Poisson's ratio as the basic elastic properties are considered, 2.7 GPa and 0.12, respectively. The elastic properties of the roof and floor rocks are also adjusted based on the variable stiffness of the loading system during the tests. A square mesh with a unit size of 0.1 m x 0.1 m was used in the pillar area. In the rest of the models, a larger rectangular mesh was used to increase the calculation speed. A list of input parameters for the calibrated model is presented in Table III.

The stress-strain curves of the pillars with the width-to-height ratios of 1:2, 2:1, and 3:1, along with their post-peak behaviour, are shown in Figure 5. To plot these curves, the stresses were recorded at the base zones of the pillars. The pillar with W/H=0.5 is weaker than other pillars. Pillars with W/H=2 and 3 are stronger and show strain hardening with localized failures before the complete collapse.

The testing process is performed by applying velocity over the upper and lower boundaries of the pillar model to increase the stress in the pillar. Note that the effect of gravity is ignored and plays no role in pillar failure. The incremental loading process via boundary

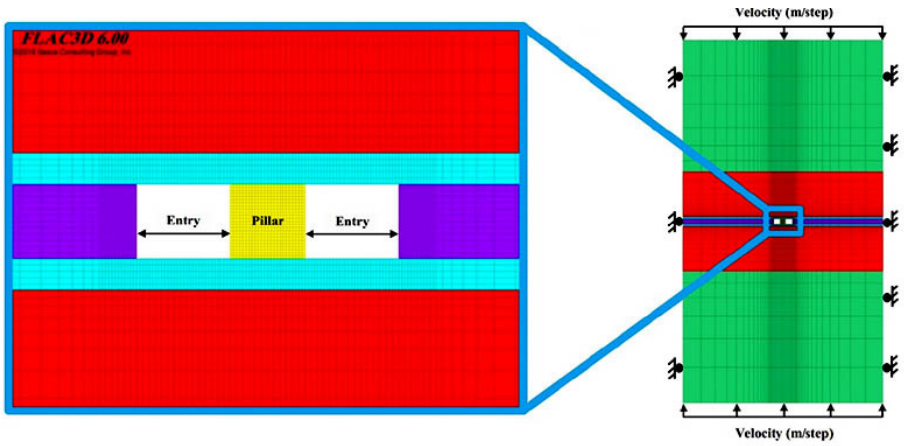

Figure 4—2D coal pillar model with details of pillar and entry

Table III

Input parameters for the calibrated Garvey model

Coal properties	
Density (kg/m³)	1313
Young Modulus (GPa)	2.7
Poisson Ratio	0.12
Initial cohesion value (Pa)	1.45 x 10^6
Cohesion drop initiating at 0.0005 plastic strain (Pa/strain)	-60 x 10^6
Residual cohesion value at 0.0213 plastic strain (Pa)	0.2 x 10^6
Initial friction angle (°)	23
Friction angle at 0.0005 plastic strain (°)	30
Residual friction angle (°)	30
Initial dilation angle (°)	2
Dilation angle at 0.0005 plastic strain (°)	10
Dilation angle from 0.0005 to 0.0213 plastic strain (°)	10
Dilation angle at 0.0218 plastic strain (°)	2
Residual dilation angle (°)	2
Tensile strength (Pa)	0.2 x 10^6
Rock mass properties	
Density of rock mass (kg/m³)	2500
Young Modulus of rockmass (GPa)	Variable (0.5;5;20)
Poisson Ratio of rock mass	0.26
Local damping coefficient	**0.8**

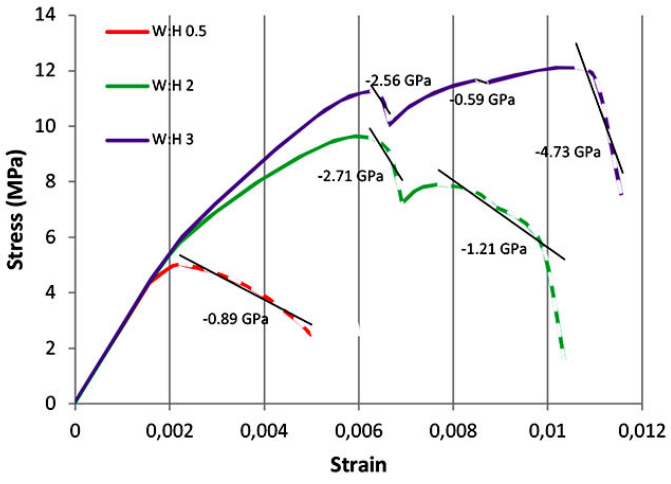

Figure 5—Stress-strain curves of coal pillars with 0.5 GPa stiffness of surrounding rock mass

displacement reduces the unstable equilibrium in the model, due to the energy released from the loading system. The velocity applied to the boundaries during each test is constant, but its value is chosen based on Young's modulus. The softer rock masses are loaded faster to reduce the time the test runs. The list of velocities applied to the model boundaries, based on Young's modulus mass values, is provided in Table IV.

Table IV

Boundary velocities relative to Young's modulus values

Rockmass E (GPa)	Boundary velocity (m/step)
0.5	40e-8
5	10e-8
20	7.5e-8

Results and discussion

The testing process is performed by applying velocity over the upper and lower boundaries of the pillar models up to the failure point. For each model, the UFI were estimated according to Equation [17]. Results of applying the proposed criterion to the pillar model with a width-to-height ratio of 1:2 for three different rock mass stiffness values are shown in the Figures 6 to 8.

In Figures 6 to 8, the UFI are higher at the corners, and lower at the top and bottom. In Figure 6, where the loading stiffness is lower than the pillar stiffness, the UFI are higher than one. This occurs in the corners and the pilar surface up to mid-height. These zones show the potential for unstable failure to occur suddenly with the release of high elastic strain energy. In Figures 7 and 8, where the loading stiffness is greater than the pillar stiffness, the UFI do not exceed one, which means that no unstable failure occurs in the pillars. For these pillars, keeping the width-to-height ratio at 1:2, the

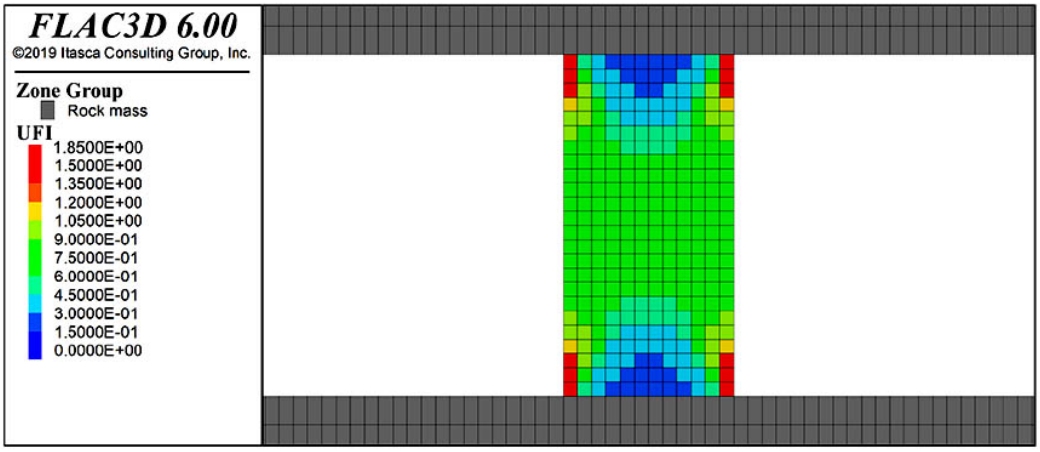

Figure 6—Result of applying the proposed criterion in a 1:2 pillar model with 0.5GPa stiffness of surrounding rock mass

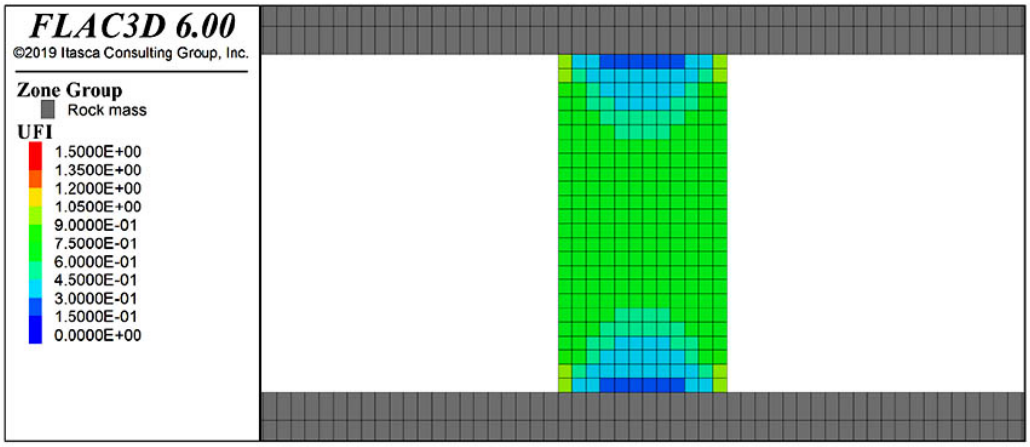

Figure 7—Result of applying the proposed criterion in a 1:2 pillar model with 5GPa stiffness of surrounding rock mass

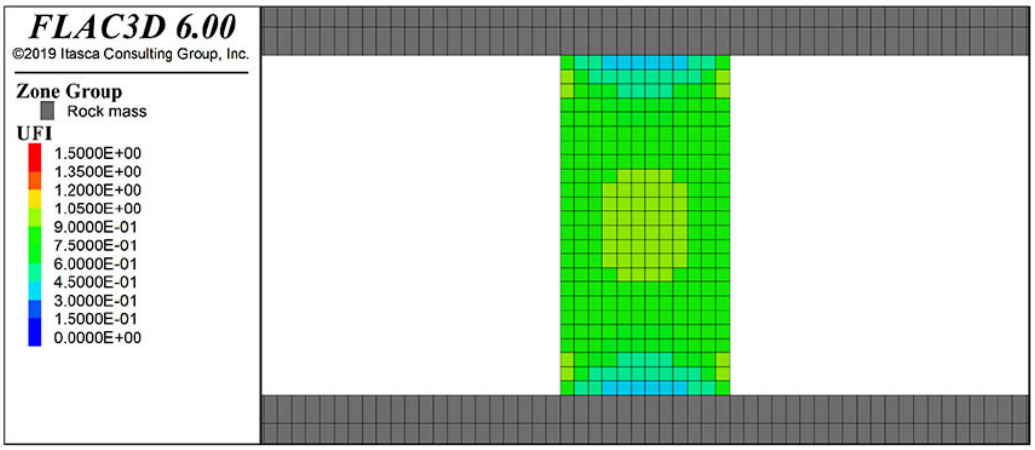

Figure 8—Result of applying the proposed criterion in a 1:2 pillar model with 20GPa stiffness of surrounding rock mass

maximum UFI value decreases with increasing Young's modulus of the surrounding rock mass, indicating the occurrence of more severe unstable failures in pillars with lower loading stiffness. By comparing Figures 6 to 8, it can be seen that, as the loading stiffness increases, the strain energy is distributed uniformly in the pillars. On the other hand, if the loading stiffness becomes less than the pillar stiffness, the strain energy is concentrated on the surface and corners of the pillar.

Figures 9 to 11 show the results of applying the proposed criterion to a pillar model with a width-to-height ratio of 2:1 for three different stiffness values of the rock mass. The UFI are higher at the corners and sidewalls, and lower at the top and bottom. Although similar results are obtained with the 1:2 pillar models, the maximum UFI decrease, which means the potential for unstable failure decreases as the width-to-height ratio increases. There is a clear difference in how strain energy is distributed in the pillar

models. It is concentrated in the walls and corners, while the centres of the pillars are less loaded. Results for the 2:1 pillar model provide a good comparison of the fracture concentration in the pillar walls. The elastic strain energy is concentrated closer to the pillar surface in Figure 9, with 0.5 GPa loading stiffness, than the pillars with 5 GPa and 20 GPa loading stiffness. In Figures 10 to 11, the energy levels are lower and are more dispersed throughout the pillar zones, and as a result, these conditions will not lead to unstable failure in the given pillar models.

Figures 12 to 14 show the results of applying the proposed criterion to the pillar model with a width-to-height ratio of 3:1 for three different rock mass stiffness values. Similar to the previous results, the concentration of elastic energy is greater at the corners and near the edges. If a failure occurred, the overall shape of the failed pillar would be similar. It is also observed that the elastic strain energy is more concentrated at the pillar ribs in the case of the 0.5 GPa rock mass. With the increase of rock mass stiffness, the energy distribution is more dispersed at the pillar.

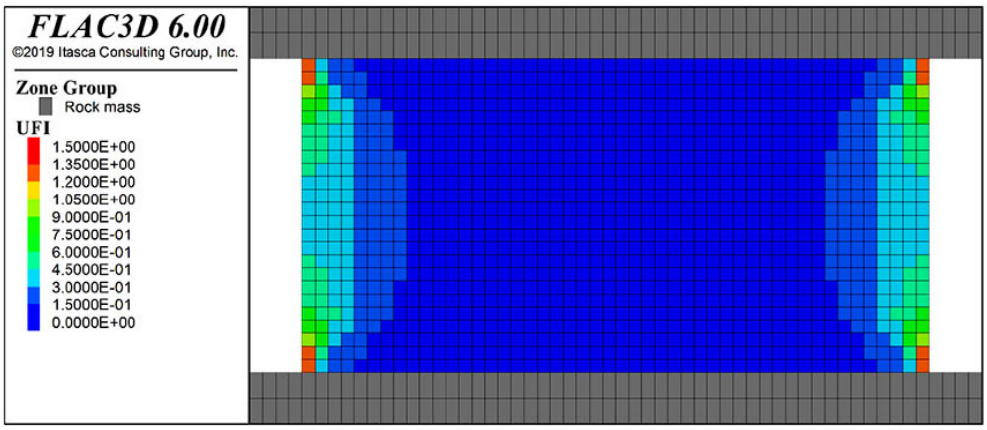

Figure 9—Result of applying the proposed criterion in a 2:1 pillar model with 0.5 GPa stiffness of surrounding rock mass

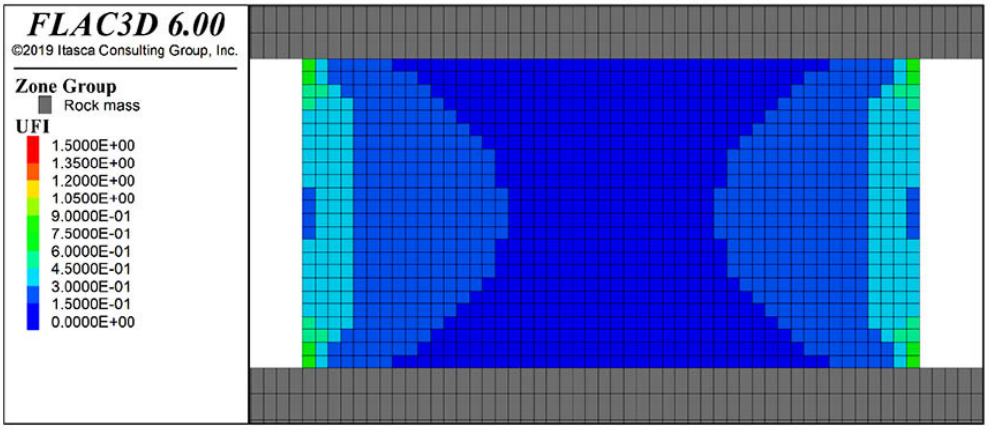

Figure 10—Result of applying the proposed criterion in a 2:1 pillar model with 5 GPa stiffness of surrounding rock mass

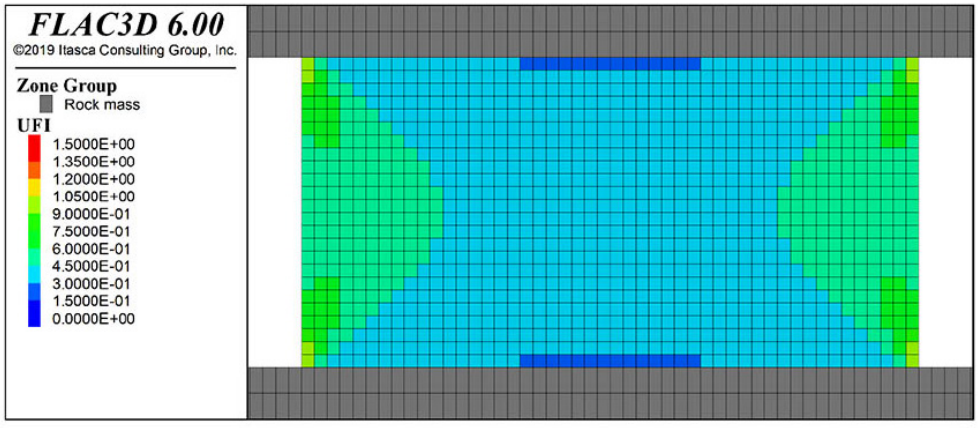

Figure 11—Result of applying the proposed criterion in a 2:1 pillar model with 20 GPa stiffness of surrounding rock mass

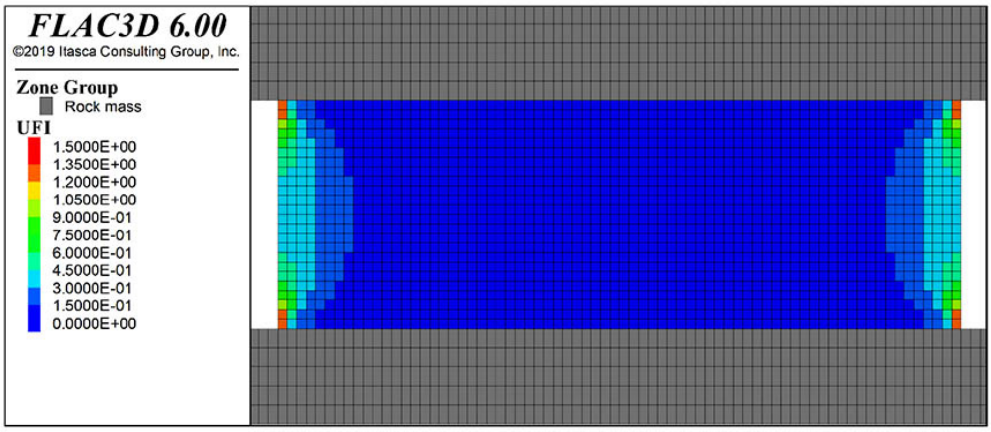

Figure 12—Result of applying the proposed criterion in a 3:1 pillar model with 0.5 GPa stiffness of surrounding rock mass

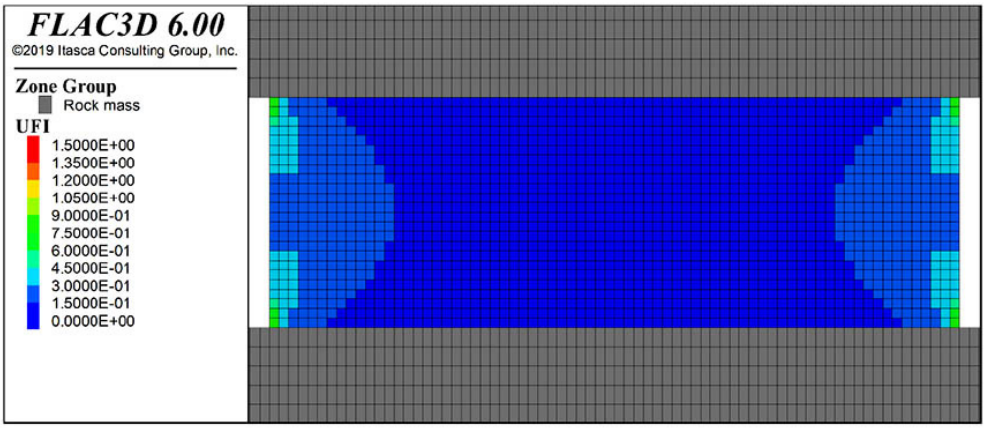

Figure 13—Result of applying the proposed criterion in a 3:1 pillar model with 5 GPa stiffness of surrounding rock mass

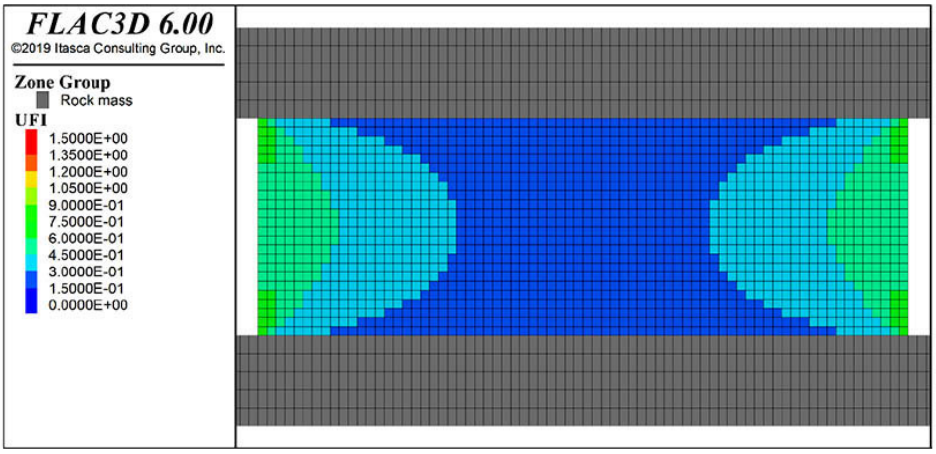

Figure 14—Result of applying the proposed criterion in a 3:1 pillar model with 20 GPa stiffness of surrounding rock mass

Figure 15 shows the maximum UFI observed in each pillar against the loading stiffness and pillar width-to-height ratio. It is seen that UFI greater than one are developed only in the coal pillars with a loading stiffness of 0.5 GPa. When the surrounding rock mass or loading stiffness increases to 5 GPa, the maximum UFI decrease to less than one for all coal pillars. From 5 to 20GPa, no further decrease in maximum UFI is observed, but a slight increase of maximum UFI is recorded, which is strange at first glance. Regarding the local failures in the stress-strain curve of coal pillars, an explanation for this issue is provided in Figure 5. Lower energy levels remain in the 2:1 coal pillar because more elastic strain energy is released compared to the 3:1 pillar. There are subtle differences in the mechanism of unstable failures in wide mining pillars.

The difference between the maximum and minimum UFI for each pillar versus loading stiffness is shown in Figure 16. How uniformly the strain energy is distributed throughout the coal pillars is revealed by the differential UFI. As the loading stiffness

increases, the strain energy is more dispersed in the coal pillars. A drastic change in energy distribution occurs when the loading stiffness changes from stiffness values lower than the pillar stiffness values to higher than the pillar stiffness values.

In Figure 17, the maximum UFI observed in each pillar are plotted against the ratio of pillar width-to-height. It is seen that the maximum UFI decrease with an increase in the width-to-height ratio. As this ratio increases, the potential for unstable failure decreases.

Based on the mining pillar models, the criterion proposed in this paper indicates that stress is concentrated in the upper and lower corners. This stress distribution pattern is also supported by a study conducted by Kabwe and Wang (2015) on the unstable failure of rock formations.

The excess energy values near the pillar edges are high, but they decrease from the surface to the depth of the model. This suggests that vertical fractures may extend layer by layer from the edges to the depth of the pillar. This result is consistent with definitions associated with unstable failure phenomena, such as spalling, slabbing, flaking, and splitting. Furthermore, this result is consistent with the experiments of Read and Martin (1996) and Hajiabdulmajid et al. (2002) in the Mine-by project regarding the simulation of the rock splitting process.

In addition, according to the above results, it is inferred that during the process of unstable failure, the rock pieces on the surface of the underground excavations may be thrown out at high speeds, and then the rock pieces behind them are thrown out at slower speeds. These results show that the instability of free surfaces of

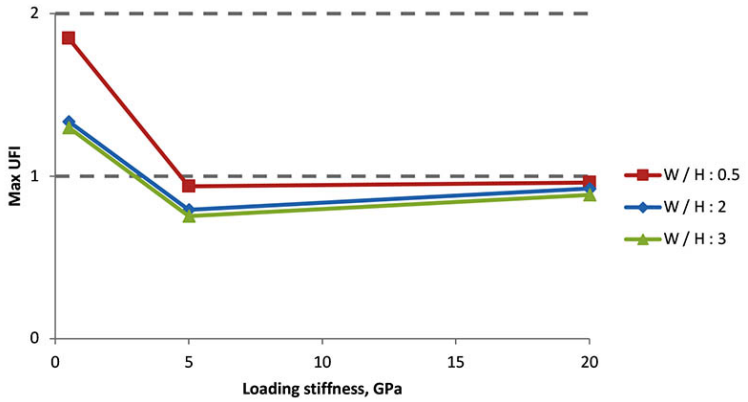

Figure 15—Maximum UFI in each pillar against the loading stiffness

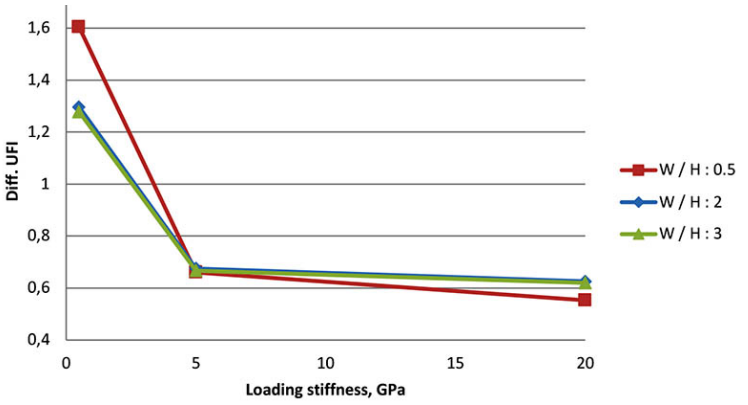

Figure—16 the differential UFI for each pillar against the loading stiffness

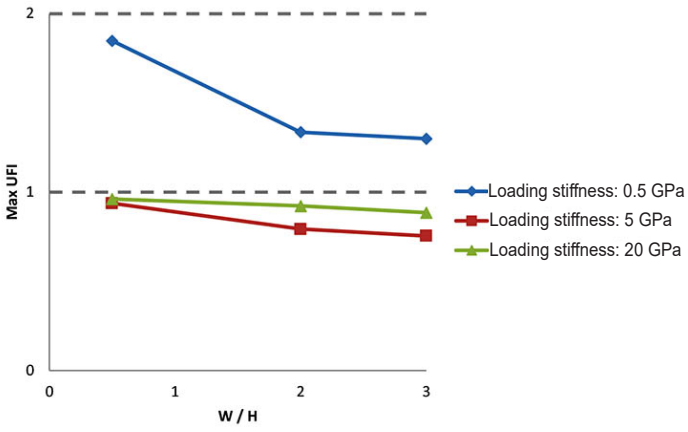

Figure 17—Maximum UFI for each pillar against the pillar width-to-height ratio

underground excavations leads to the initiation of unstable failure. Therefore, it is suggested to quickly reinforce all exposed surfaces with shotcrete and bolts after excavating the rock. These results are consistent with the numerical studies of Sun et al. (2007) on the simulation of rock bursting in circular tunnels under unloading conditions.

Conclusions

So far, many efforts have been made to reduce the probability of unstable failure events by modern mining operations. It is hard to completely prevent the phenomenon of unstable failure in mining practice, due to the uncertain stresses, strains, and micromechanical characteristics of the surrounding rocks. The application of numerical methods is essential in reducing the destructive effects of unstable failure in underground excavations, although the existing procedures for analysing this type of failure in numerical models also have limitations.

A method was developed to identify the location and intensity of unstable rock failure resulting from unstable equilibrium in continuous numerical models. Static energy balance was used to calculate the values of elastic strain energy and to develop a criterion to determine the areas prone to unstable failure initiation in mining pillars. The procedure of energy calculation as a direct method in the analysis of unstable failure compared to other presented approaches, has more physical relevance in the field of rock mechanics, providing a better understanding of the phenomenon of unstable fracture. In general, the proposed criterion performed well in identifying the fracture initiation regions and was consistent with previous studies on unstable rock failure.

The technique developed in this study can be used as a tool to assist future research on the design of mining pillars under unstable failure conditions, the selection of support systems, the evaluation of cutting sequences in retreat mining, the study of stress relaxation techniques, and the back analysis of unstable rock failures. This technique can help predict the occurrence of such incidents and control the resulting physical and financial damage.

References

Askaripour, M., Saeidi, A., Rouleau, A., Mercier-Langevin, P. 2022. Rockburst in underground excavations: A review of mechanism, classification, and prediction methods, *Underground Space*, vol. 7, no. 4, pp. 577–607. https://doi.org/10.1016/j.undsp.2021.11.008

Bacha, S., Mu, Z., Javed, A., Al Faisal, Sh. 2020. A review of rock burst's experimental progress, warning, prediction, control and damage potential measures. *Journal of Mining and Environment (JME)*, vol. 11, no. 1, pp. 31–48. https://dx.doi.org/10.22044/jme.2019.9092.1797

Badr, S.A.E. 2004. Numerical analysis of coal yield pillars at deep longwall mines. PhD Thesis, Colorado School of Mines, Golden, CO, USA.

Barton, N., Lien, R., Lunde, J. 1974. Engineering classification of rock masses for the design of tunnel support. *Rock Mechanics and Rock Engineering,* vol. 6, no.4, pp. 189–236.

Brady, B.H.G., Brown, E.T. 2007. *Rock mechanics: for underground mining*. 3rd ed. Springer.

Chase, F.E., Zipf, R.K., Mark, C. 1994. The massive collapse of coal pillars: case histories from the United States. *13th International Conference on Ground Control in Mining.* West Virginia University, Morgantown, pp. 69–80.

Cook, N.G.W. 1965. The failure of rock. *International Journal of Rock Mechanics and Mining Sciences & Geomechanics Abstracts,* vol. 2, no. 4, pp. 389–403.

Garvey, R.J. 2013. A study of unstable rock failure using finite difference and discrete element methods. PhD Thesis, Colorado School of Mines. Golden, CO, USA.

Hajiabdolmajid, V., Kaiser, P.K., Martin, C.D. 2002. Modelling brittle failure of rock. *International Journal of Rock Mechanics and Mining Sciences*, vol. 39, no. 6, pp. 731–741.

Hobbs, B.E., Ord, A. 1989. Numerical simulation of shear band formation in a frictional-dilational material. *Archive of Applied Mechanics,* vol. 59, no. 3, pp. 209–220.

Hoek, E., Brown, E.T. 1980. Underground excavation in rock. *The Institute of Mining and Metallurgy*, London, UK.

Itasca Consulting Group Inc. 2018. FLAC3D (Fast Lagrangian Analysis of Continua in 3 Dimensions), Version 6.00. Minneapolis, MN, USA.

Kabwe, E., Wang, Y. 2015. Review on Rockburst Theory and Types of Rock Support in Rockburst Prone Mines. *Open Journal of Safety Science and Technology*, vol. 5, no. 04, pp. 104–121. http://dx.doi.org/10.4236/ojsst.2015.54013

Kidybinski, A. 1981. Bursting liability indices of coal. *Journal of Rock Mechanics and Mining Sciences*, vol. 18, pp. 295–304.

Neyman, B., Szecowka, Z., Zuberek, W. 1972. Effective methods for fighting rock burst in Polish collieries. *5th International Strata Control Conference.* London, pp. 1–9.

Osterwald, F.W. 1962. USGS relates geologic structures to bumps and deformation in coal mine workings. *Mining Engineering,* vol. 14, pp. 63–68.

Peperakis, J. 1958. Mountain bumps at the sunnyside mines. *Mining Engineering*, vol. 211, pp. 982–986.

Read, R.S., Martin, C.D. 1996. Technical summary of AECL's Mine-by Experiment phase I: Excavation response. *Report no. AECL–11311,* Atomic Energy of Canada Ltd. Pinawa, MB, Canada.

Russenes, B.F. 1974. Analysis of rock spalling for tunnels in steep valley sides. M.Sc. thesis, *Norwegian Institute of Technology*, Trondheim, Department of Geology, 247p. (in Norwegian).

Salamon, M.D.G. 1970. Stability, instability and design of pillar workings. *International Journal of Rock Mechanics and Mining Sciences & Geomechanics Abstracts*, vol. 7, no. 6, pp. 613–631.

Sun, J., Zhu, Q., Lu, W. 2007. Numerical simulation of rock burst in circular tunnels under unloading conditions. *Journal of China University of Mining and Technology*, vol. 17, no. 4, pp. 552–556. https://doi.org/10.1016/S1006-1266(07)60144-8

Tao, Z.Y. 1988. Support design of tunnels subjected to rockbursting. *ISRM International Symposium, Rock Mechanics and Power Plants*, A.A. Balkema, pp. 407–411.

Wang, X.M., Dong, L.J., Fu, Y.H. 2009. Prediction of possibility and the level of rockburst based on uncertain average graded analysis method. *Scientific Technical Review,* vol. 27 no. 18, pp. 78–81. http://www.kjdb.org/EN/Y2009/V27/I0918/78

Zhang, G., Chen, J.X., Hu, B. 2003. Prediction and control of rockburst during deep excavation of a gold mine in China. *Chinese Journal of Rock Mechanics and Engineering* vol. 22, no. 10, pp. 1607–1612. https://wenku.baidu.com/view/4e92c4d076a20029bd642d10.html

Zhao, G., Wang, D., Gao, B., Wang, S. 2017. Modifying rock burst criteria based on observations in a division tunnel. *Engineering Geology*. vol. 216, pp. 153–160. https://doi.org/10.1016/j.enggeo.2016.11.014

Zhou, J., Li, X.B., Mitri, H.S. 2017. A critical survey of empirical methods for evaluating rockburst potential. *15th IACMAG*, Wuhan, China.

Zhou, J., Zhang, Y., Li, C., He, H., Li, X. 2024. Rockburst prediction and prevention in underground space excavation. *Underground Space.* vol. 14, pp. 70–98. https://doi.org/10.1016/j.undsp.2023.05.009

Zingano, A.C., Koppe, J.C., Costa, J. 2004. Violent coal pillar collapse–a case study. 23rd *International Conference on Ground Control in Mining*, Peng, Khair and Heasley Ed., West Virginia University, Morgantown, USA. ◆